AFML-TR-76-81

/2

B.S.

DEFECT-PROPERTY RELATIONSHIPS IN COMPOSITE MATERIALS

VIRGINIA POLYTECHNIC INSTITUTE AND STATE UNIVERSITY
BLACKSBURG, VIRGINIA

APRIL 1976

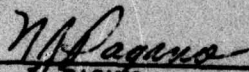TECHNICAL REPORT AFML-TR-76-81

D D C

RECEIVED

NOV 10 1976

B

AIR FORCE MATERIALS LABORATORY
AIR FORCE WRIGHT AERONAUTICAL LABORATORIES
AIR FORCE SYSTEMS COMMAND
WRIGHT-PATTERSON AIR FORCE BASE, OHIO 45433

N. J. PAGANO
Project Engineer

FOR THE DIRECTOR

S. W. TSAI, Chief
Mechanics and Surface Interactions Branch
Nonmetallic Materials Division

REPORT DOCUMENTATION PAGE	READ INSTRUCTIONS BEFORE COMPLETING FORM

1. REPORT NUMBER	2. GOVT ACCESSION NO.	3. RECIPIENT'S CATALOG NUMBER
AFML-TR-76-81		

4. TITLE (and Subtitle)	5. TYPE OF REPORT & PERIOD COVERED
DEFECT PROPERTY RELATIONSHIPS IN COMPOSITE MATERIALS	Annual Report. 3 Feb. 1975 - 3 Jan. 1976.
	6. PERFORMING ORG. REPORT NUMBER

7. AUTHOR(s)	8. CONTRACT OR GRANT NUMBER(s)
K. L. Reifsnider E. G. Henneke W. W. Stinchcomb	F33615-75-C-5119

9. PERFORMING ORGANIZATION NAME AND ADDRESS	10. PROGRAM ELEMENT, PROJECT, TASK AREA & WORK UNIT NUMBERS
Virginia Polytechnic Institute & State University Engineering Science and Mechanics Department Blacksburg, VA 24061	735003A1

11. CONTROLLING OFFICE NAME AND ADDRESS	12. REPORT DATE
Air Force Materials Laboratory (AFML/MBM Air Force Systems Command Air Force Wright Aeronautical Laboratories Wright-Patterson AFB, Ohio 45433	Apr. 1976
	13. NUMBER OF PAGES
	53

14. MONITORING AGENCY NAME & ADDRESS(if different from Controlling Office)	15. SECURITY CLASS. (of this report)
52p.	Unclassified
	15a. DECLASSIFICATION/DOWNGRADING SCHEDULE

16. DISTRIBUTION STATEMENT (of this Report)

Approved for public release; distribution unlimited.

17. DISTRIBUTION STATEMENT (of the abstract entered in Block 20, if different from Report)

18. SUPPLEMENTARY NOTES

19. KEY WORDS (Continue on reverse side if necessary and identify by block number)

Composite Materials, Graphite-epoxy, Defects, Properties, First Ply Failure, Nondestructive Testing, Delamination, Cracking

20. ABSTRACT (Continue on reverse side if necessary and identify by block number)

This report describes the initial results of an investigation which has as its objectives the determination of the nature of damage in two graphite-epoxy (GEp) laminates under various combinations of loading as completely and precisely as possible, and the investigation of the corresponding mechanical property changes. The results include several new findings, the development of unique investigative methods, and substantial deviations from the predictions of common models.

DD FORM 1473 EDITION OF 1 NOV 65 IS OBSOLETE
1 JAN 73

404722

PREFACE

This investigation is the initial work of a program which is being carried out at Virginia Polytechnic Institute and State University under Contract F33615-75-C-5119 to the Air Force Materials Laboratory, Wright-Patterson Air Force Base. The technical monitor is Dr. N. J. Pagano.

The investigation was carried out between 3 February, 1975 and 3 February, 1976.

ACCESSION for

NTIS	White Section	☑
ODC	Buff Section	☐
UNANNOUNCED		☐

JUSTIFICATION..............................

....

BY..
DISTRIBUTION/AVAILABILITY CODES

Dist.	AVAIL and/or SPECIAL
A	

TABLE OF CONTENTS

LIST OF ILLUSTRATIONS

LIST OF TABLES

SECTION I

INTRODUCTION

It can be said that science and engineering are at roughly the half-way mark in their development of an understanding of materials response. While accurate descriptions and understanding of the response of ideal materials have been achieved in many cases, the development of understandings of the non-idealities of real materials which usually has to do with their engineering life and the nature of their failure is very much in its infancy. This is especially true of composite materials. For these materials, even the ideal response is nonuniform and anisotropic. Development of damage is still less ideal, and can not be treated as an obvious extension of descriptions of related phenomena in homogeneous materials (such as self-similar through-crack propagation for example.)

While experimental data of one type or another abounds, analytical speculation is even more abundant. Discretion forebids a complete listing of either set of efforts here. Instead, some general categorizations will provide context for the work to be presented below. There is a fairly large group of efforts centered around the linear elastic fracture mechanics discipline with various corrections for such things as heterogeneity and the lack of local (at least) self-similarity. Wu, for example, introduces, among other things, a set of crack surface forces to account for unbroken fibers as the crack progresses.[1] The principal aim of these characterizations is to determine a correct field stress intensity relationship which has a critical value which is a material characteristic and can be used as a one-parameter characterization of the material toughness. A review of these types of activities has been given by Smith.[2]

A somewhat more complete attempt to deal with the specific details of

1

the local mechanics of damage development is typified by an approach pursued by Rosen and co-workers.[3] They developed a model which included a three-zone idealization of the region surrounding a flaw (hole or crack). The 0° plies were used as a basis for the analysis: the influence of the angle plies was included by introducing a transverse reinforcing factor. The principal advantage of this type of approach appears to be the rather large number of adjustable parameters which can be selected and "calibrated" by laboratory experience. The flexibility assists in the description of behavior but may provide little if any aid to the effort to explain the behavior.

Of course, numerous design-oriented models also exist. The aim of these models is not to provide a phenomenological explanation but to provide empirical relationships which relate and predict design parameters. One such model, which is widely used in various forms, was set forth by Halpin, et. al.[5] Their model is a wear-out model which attempts to characterize the characteristic strength and statistical distribution of strength as a function of damage. The analytical basis of the model is a Weibull distribution representation of static strength which, according to the model, is related to the distribution of strength after damage. The two assumptions that are basic to the model are that these materials fail as a consequence of growth to instability of pre-existing flaws which are statistically distributed, and that those initial flaws grow deterministically in a manner controlled by the material state and environmental history.[6]

The single most obvious shortcoming of all of the characterization efforts mentioned above is that they are not theories based on theorems derived in a pragmatic way from a complete set of laws or first principals known to represent the essential details of the material behavior. This is true mainly because a proper understanding of damage development and its' consequences has not been

2

developed from experimental investigations. The need for such an understanding has motivated the present work.

The objects of the present investigation are to determine the nature of damage in two types of graphite-epoxy (GEp) laminates as completely and precisely as possible and to investigate the corresponding mechanical property changes for various combinations of loading. Our initial approach has been an experimental investigation by a variety of methods, some of which are unique to our laboratories and were developed for the purpose of the present investigation. For purposes of context and comparison, some analysis using established methods was carried out, including a laminate analysis of ply stresses including residual thermal stresses, and an appropriate analysis of through the thickness normal stresses. These results are also reported. Finally, some preliminary conclusions are drawn.

SECTION II

TECHNIQUES AND EQUIPMENT

To carry out the stated objectives of this investigation, an experimental program was designed to carefully study the development of damage in the GEp laminates using special nondestructive investigation (NDI) methods such as real-time thermography, ultrasonics, x-radiography, and light and scanning electron microscopy. These methods, when used in concert with more conventional testing techniques such as static loading and cyclic loading, form the foundation of the experimental investigation and are briefly described below.

1. Quasi-Static Testing

Tension tests, using incremental and continuous loading, were conducted on a 20 kip Instron machine at a crosshead displacement rate of 0.05 inches

3

per minute. Strains were measured using axial strain gages mounted on the middle of the specimen surface and transverse strain gages mounted at the free edge. A light microscope was adapted to a specially designed fixture to provide X, Y, and Z translation of the microscope while attached to the movable crosshead of the testing machine. The specimen is positioned in the load frame so that the observer looking through the microscope views the edge of the specimen under load and scans along the length to detect defects which initiate during loading and to follow their growth.

The test specimen is also instrumented with an ultrasonic transducer for attenuation measurements under load. Changes in attenuation of ultrasonic energy due to the initiation and growth of defects are recorded on a strip chart recorder for correlation with load and strain data.

A video-tape camera with close-up lens has also been employed on occasion to record the damage history of the specimens under load for later study and analysis.

Two kinds of quasi-static loading tests have been conducted. In one, the specimens are loaded incrementally to failure. An initial load of approximately 500 pounds is applied and the edge of the specimen is scanned through the microscope to observe any defects which may have developed. If cracks are found, the load is incremented in 100-200 pound steps with additional microscopic observations and photographs made at each level to document the behavior of the defects. If no cracks or delaminations are observed at the initial load level, the load is increased to 800 pounds and the scanning continued.

The second kind of test subjects a specimen to continuous loading to an intermediate damage state ($\sigma \approx 0.4\ \sigma_u$). The specimen is then scanned as described above and records are made of the damage (crack density, locations,

4

lengths). The load is then removed and the specimen is moved to an MTS
machine for dynamic testing to study the nature of the damage under combin-
ations of static-dynamic loading.

2. Fatigue Testing

An MTS servo-controlled, closed-loop, tension-torsion testing machine
was used for the fatigue loading tests. The machine has an axial capacity
of 50,000 pounds, and a torsional capacity of 20,000 in-lbs. The torsional
control mode was used to prevent twisting of the specimens. The control
unit of the machine can be used to monitor load, strain, and displacement
continuously during cyclic loading. For the elongation range of the
specimens used in this program, the upper response limit of the machine is
50-60 cycles per second. The specimens were held by means of a set of Instron
20,000 pound wedge grips. The grip faces were coated with epoxy to avoid
abraiding the specimen surfaces. In instances where tabs were not used on
the specimens, the specimen ends were wrapped with medium grit emery paper
a method which was very effective in assuring proper gripping with only
occasional failures in the grip regions.

The test and response parameters were monitored by a Tektronix DPO
3107 data acquisition system. The system continuously sampled load, strain
and (when used) acoustic emission count, and calculated stress, dynamic
stiffness, energy dissipated, and specific damping ratio. The system also
calculates and displays the hysteresis loop. This on-line system is com-
pletely automatic and does not require operator supervision or alteration
of the test.

3. Ultrasonic Pulse-Echo Method

The ultrasonic pulse-echo technique was used to follow the development

5

of damage in the composite by measuring the attenuation of the ultrasonic pulses. In the usual case, it is assumed that the amplitude of the ultrasonic pulse decays according to the relation

$$A = A_0 e^{-\alpha x} \qquad (1)$$

where α is a positive, real number independent of x and is called the attenuation coefficient. This definition will have to be modified in the future to apply to the technique discussed below using a delay block. However, for the present report, we will assume an attenuation to be defined in the form of Eqn. (1). For brevity, α shall be referred to as simply the attenuation in the sequel. Experimentally, α can be measured by determining the amplitude of each echo in the pulse-echo train, plotting this data on a semi-logarithmic plot versus distance traveled, and determining the slope of the resulting straight line. Indeed, this technique proves the degree of validity of the assumption of equation (1) by the degree of "straightness" of the plot.

The units of the attenuation coefficient are expressed in terms of either nepers per unit length or decibels per unit length. One neper is that attenuation which causes an amplitude to be reduced to a value 1/e of its original value (1 neper = $\log_e \frac{A_0}{A} = \log_e e = 1$) and one decibel is defined as that attenuation which reduces the amplitude to $10^{-1/20}$th that of its original value (1db = $20 \log_{10} \frac{A_0}{A} = 20 \log_{10}(10)^{1/20} = 1$). Thus α is expressed in nepers per unit length or in decibels per unit length by

$$\alpha = \frac{1}{x_2 - x_1} \log_e \frac{A_1}{A_2} \text{ nepers/unit length}$$

$$\alpha = \frac{1}{x_2 - x_1} 20 \log_{10} \frac{A_1}{A_2} \text{ db/unit length}$$

6

In what follows, the units of db/echo will be used. The latter results from a slight change in definition to fit the pulse echo method. Since each echo corresponds to one round-trip in the specimen, which of course is a fixed distance, the factor $1/(x_2-x_1)$ can be modified to read $1/n(2L)$ where L is the specimen length and n is the number of echoes between amplitudes A_1 and A_2.

The pulse-echo technique used in the present work was a modified delay block approach. The transducer was bonded to the specimen with stop-cock grease and a quartz delay block, approximately 1 inch in length, was bonded to the other side of the specimen, again with stop-cock grease. The ultrasonic pulse thus made a trip through specimen, delay block, and specimen again before being monitored and displayed as an echo. The thinness of the specimen necessitated the use of the quartz delay block so that sufficient time separation could be obtained to distinguish the echos as separate pulses on the oscilloscope. The quartz block was chosen so that the attenuation of the pulse in it is relatively small. In any case, since the delay block does not change during a test, any change in attenuation is attributable to changes in the specimen. A C-clamp was used to hold the transducer-specimen-delay block combination together in the testing machine (Fig. 1). It should be noted that this technique then allows for real time attenuation measurement while a load, either static or fatigue, is applied to the specimen. However, the technique is presently restricted to being able to monitor only that volume of the specimen immediately under the transducer. Additional modifications would have to be made to allow for scanning the length and width of the specimen.

Two techniques were employed to determine the attenuation changes during the year's work reported here. One technique required extensive laboratory development time and the second required the purchase of a new item of equip-

ment. The first method employed use of the digital processing oscilloscope (DPO) together with appropriate software written for the desk calculator which interfaces with the DPO. For this method, the DPO digitizes the ultrasonic echos. In order to make the method as sensitive as possible, each echo must be time-delayed and displayed one at a time on the scope. By doing this, each echo will be digitized by the maximum number of points so that a better value of the maximum amplitude is obtained. This value of the maximum amplitude is then plotted on a semi-logarithmic plot versus the number of echoes, and a least squares straight-line fit is made to the data points. The slope of this line is the attenuation per echo as defined above. A typical example is given in Fig. 2. This method has the advantage of obtaining an attenuation value which is averaged over several returning echoes by a least-squares routine. Also, by plotting both the least-squares fit and the data points, one can see how closely the attenuation approximates an exponential decay. The method has a major disadvantage in that significant amounts of time are required to have a technician place each echo on the scope, to have the calculator search through the memory to find the maximum amplitude, and to have the calculator fit and plot a least-squares line to the data. After several iterations, the method was developed to a point where the time required was reduced to 30 seconds. Even with this, it is necessary to stop the test and to hold the displacement constant during this interval to obtain the attenuation value at the given load level. At best then only a discrete number of attenuation data points can be obtained as a function of load. Also, as will be pointed out later in the results, the attenuation may continue to change even under constant displacement, thereby making the comparison of amplitudes of different echoes questionable by the time all echoes have been separately stored by the DPO.

8

The second technique used to determine attenuation utilizes a Matec Attenuation Recorder, Model 2470A, an item of equipment which was purchased by the Virginia Polytechnic Institute and State University in direct support of the effort reported here. This instrument electronically compares the peaks of two echoes which are operator selected and outputs this comparison directly as attenuation in db per echo for chart recording. This instrument will update the attenuation measurement approximately once each second. Thus, the outstanding advantage in using this instrument is that real-time attenuation data can be taken during either static or fatigue loadings. The disadvantage is that only two echoes are compared, losing the ability to average over several echoes. Several cross checks were made on unloaded specimens to check the attenuation results obtained from the DPO averaging technique and from the Matec recorder. In all cases the difference between the attenuation values obtained by the two methods was negligible. Hence, it is felt that a good level of confidence can be placed in the data obtained from the Matec recorder even though only two echoes are used. This instrument was used to obtain continuous recording of ultrasonic attenuation through entire loading sequences as reported below.

4. Acoustic Emission

Standard acoustic emission tests were run on several specimens. Because these tests are standard, there is no need to detail them here. These tests consisted of using transducers to monitor emission events by counting every vibration peak above a set trigger level. The counter used in these tests has a highly stable and accurately set trigger level. The counts per second were plotted on a y-time recorded for later synchronization with load and strain data.

9

5. Thermography

Part of the original test program called for the use of thermography to study the development of damage by the emission of heat patterns. The release of heat is based upon the concept that as damage occurs in a localized region, the strain energy in the neighboring material will be released. While some of this energy release is used to create new surfaces or to propagate stress waves away from the region, a substantial amount will be locally released as heat. All of the details of the heat which is released are directly related to the damage event. The seriousness of the defect can be determined by the amount of heat released. The position and spatial distribution of the heat emission specifies the extent of damage. Thus, if this information is collected in a time-resolved fashion, the propagation and propagation rate of damage can be determined.

The measurement of time-resolved heat emission requires some very special instrumentation. An AGA 680 video-thermography camera was used in this investigation. This instrument is the most sensitive of its kind available, having temperature discrimination of 0.2° C. It is time-resolved, displaying a video picture once every 1/16 sec. Both black-and-white and color monitors were used in this study. The black-and-white monitor gives continuous gray shading of the heat pattern and has available two isotherms which can be continuously varied over the set temperature scale. The color monitor displays ten different colors, each corresponding to a relative temperature range of 1/10 of the set maximum temperature scale.

In order to see a damaged region, it has been found necessary at present to put some steady state energy into the specimen. The earlier thermography work performed at this laboratory studied heat emission patterns during fatigue loading of composite specimens. The cyclic loading cycles served as a steady

10

source of energy which was observed to be preferentially dissipated at the damaged regions. As suggested above, the extent and propagation rate of the damage could easily be followed by the increasing intensity and distribution of the heat patterns. For quasi-static loadings, the progression of damage has not as yet been amenable to observation by the thermographic technique.

Because of this, a new technique has been conceived and is being studied at this laboratory. We have chosen to call this technique Vibrothermography because it utilizes high frequency vibrations to delineate damaged regions by preferential heat pattern development and thermography to visualize these heat patterns. The concept is based upon our observations of the fatigue loaded specimens and upon the suggested idea that steady state vibrations should interact differently with damaged regions than with un-damaged ones. Currently, vibrations are being introduced into a specimen by mounting one end on a shaker. This shaker is then operated over a narrow frequency range of approximately 1000 - 2000 HZ. The vibration amplitudes that result in the specimen have not as yet been measured, but are small. As a qualitative statement, the vibrations can be felt by hand but can not be seen.

The further development of vibrothermography is compelling for several reasons. First, since the interaction of stress waves with locally damaged regions will vary with wave length, it is currently believed that the size of damaged regions may be studied by sweeping the vibrations through a broader frequency range. Second, by developing an analytical model to relate heat emission to local stress fields, the type or mode of damage may be delineated. Third, it is easy to foresee that vibrothermography may be developed into a field technique whereby one might introduce vibrations into a structure by a hand held ultrasonic horn or other suitable instrument and detect damage by a thermographic camera.

11

6. Microscope Examinations

Several types of microscopic examinations were performed. A standard microscope was mounted on a translation stage which, in turn, was mounted on the crosshead of the quasi-static (tensile) testing machine so that observations of crack formation and development could be made at load during specimen testing. The magnification possible with that arrangement was a maximum of approximately 80X. A bench metallograph was also used for both high and low magnification examinations. The metallograph had a practical limit of about 900X magnification. In addition, the metallograph was capable of dark field illumination and polarized light illumination, two important capabilities which were very helpful in the determination of the nature of the details observed.

The highest magnification observations were made by means of an AMR Model 900 scanning electron microscope. Magnifications up to four or five thousand were used to reveal the local nature of such things as delamination and transverse cracking. Because of the roughness of the specimen surfaces and the difficulty in obtaining any type of polished surface on such materials, the scanning electron microscope was a valuable tool for microscopic examinations, especially when specific details of the behavior of the constituent materials individually were of interest.

SECTION III
RESULTS

1. Materials and Specimens:

The material used in this investigation is Hercules Type A/S 3501-5 graphite-epoxy prepreg. Unidirectional quality control tensile specimens were tested to failure and the properties reported by the manufacturer.

Laminate mechanical properties and physical properties for two panels are reported in Table I.

Panels of A/S 3501 GEp were laid-up in two quasi-isotropic configurations and cut into 1" x 7" strips. Type I specimens have a geometry of $(0^0, \pm 45^0, 90^0)_s$ and Type II specimens have a $(0^0, 90^0, \pm 45^0)_s$ stacking sequence. A major difference in the response of the two types of specimens is due to the distribution of the through-the-thickness normal stresses (σ_z) near the free edge when an axial tensile load is applied. Type I specimens develop tensile stresses in this region whereas compressive through-the-thickness stresses are produced in all but the 0^0 ply in Type II specimens (Fig. 3). All specimens have 2" glass epoxy end taps which taper at the gage section.

The Type I specimens were divided into two sub-groups. Type IA specimens have an initial curvature corresponding to a residual strain distribution from +500 μ in./in. to -500 μ in./in. through the thickness. It is suspected that the curvature is due to non-symmetrical heat sinks during the curing process. Type IB specimens have no initial curvature. Some average mechanical properties for the specimens are given in Table II.

2. Laminate Analysis:

A laminate analysis was performed on these two configurations to provide reference information for interpretative purposes. The material properties used in the analysis appear in Table III. The results of the analysis were used to predict a stress-strain curve and were combined with several types of failure criteria to determine the failure mode predictions of the elementary theory.

The laminate analysis results predict the stress-strain curve shown in Fig. 3. The predicted laminate stiffness is 7.73 x 10^6 psi for the initial portion of the curve. Using a maximum strain criterion, failure of the 90^0

TABLE I

ROOM TEMPERATURE MATERIAL PROPERTY DATA
TYPE AS/3501 GRAPHITE EPOXY

Property	Type I[1]	Type II[2]
Average 0° Tensile Strength (KSI)	232	225
Average 0° Tensile Modulus (MSI)	20.0	19.4
Fiber Volume (%)	63.8	60.4
Resin Content (%)	28.87	31.95
Density (lb/in.^{3})	0.0577	0.0570
Void Content (%)	0.13	0.04
Ply Thckness (in.)	0.0054	0.0054

(1) Panel No. 2206
(2) Panel No. 2506

TABLE II

AVERAGE MECHANICAL PROPERTIES OF
GRAPHITE EPOXY LAMINATES

Property	Type IA	Type IB	Type II
Elastic Modulus (MSI)	6.6	6.8	6.1
Tensile Strength (KSI)	72.6	65.8	70.5
Fracture Strain (μ in/in)	11,700	10,400	11,400

14

TABLE III

SUMMARY OF PROPERTIES *
FOR AS-3501

Elastic Stiffness Properties	Tensile Value	Compression Value
E_1	20.2×10^6 psi	17×10^6 psi
E_2	1.4×10^6 psi	1.6×10^6 psi
ν_{12}	0.28	0.28
G_{12}	0.65×10^6 psi	0.65×10^6 psi

Strength Properties

X	235,000 psi	180,000 psi
Y	8,200 psi	25,000 psi
S	17,900 psi	17,900 psi

Other Properties

Thermal expansion coefficients:

α_1 (fiber direction) = -0.2×10^6 in/in/°F

α_2 (transverse direction) = 13.0×10^{-6} in/in/°F

Fiber volume fraction 0.62

Ply thickness 0.0052 ± 0.0004 in.

Void content 2%

Density 0.057 lb/in^3

Stress-free temperature 278°F

* Data Supplied by Hercules, Inc.

15

plies is predicted at about 950 lb. load or a stress of 18 ksi. The details of the analysis are briefly described in Appendix A. At the failure point of the 90^0 plies a change of a few percent in the laminate stiffness is predicted. The ultimate strength of the laminate, predicted by a Tsai-Hill analysis, was found to be 76.5 ksi if thermal residual stresses were ignored or 77.7 ksi when thermal stresses were included in the analysis. The inclusion of the thermal residual stresses is important because of its magnitude of influence in some cases, but somewhat imprecise since exact representations of the material behavior have not been established. Careful study of the problem, however, has been made by Pagano, et. al.[7]

Although Type I and Type II laminates were both quasi-isotropic, there is a great difference between the through the thickness or z stress distributions. To establish the nature of those distributions, the laminate analysis was combined with the approach of Pagano and Pipes.[8] Normal stresses in the z direction were of primary concern because of the possibility of delamination in the instance that σ_z is positive. The σ_z stresses are determined by the moments caused by σ_y (transverse) stresses in the plane of the laminate. The σ_y distribution for the Type I laminate layup is shown in Fig. 5. The thermal residual stresses are shown by the solid curve and the broken curve represents the total stresses due to the thermal residual stress plus a 1 kip axial load. In general, there is a tensile y stress in the outer three layers and compressive stress in the 90^0 ply next to the centerline of the specimen. The σ_z distribution which results for this layup is shown in Fig. 6. Again, the solid curve is the thermal residual stress and the broken curve represents the values when an axial load of 1 kip is applied. The σ_z values are tensile throughout the thickness. At an applied load of 1 kip the tensile stress at the interface between the 90^0 and -45^0 ply reaches a value of about 10 ksi which should

16

initiate delamination if a simple maximum stress criterion is applied. If it is argued that thermal residual stresses are relaxed near the specimen edge (for which these plots apply), then delamination may occur at a higher load. However, a load of at least 1000 lb. (an applied stress of at least 23 ksi) should be required to initiate delamination in these specimens.

The situation for the Type II specimens is quite different. The σ_y distribution is shown in Fig. 7. The curves have the interpretations described above. The 90° ply has been moved to the first underlayer position to attempt to induce a moment which has opposite sense to that of the Type I laminate. Fig. 8 shows the resultant σ_z distribution. The thermal residual stresses are small and inconsequential. When a 1 kip load is applied the laminate develops only compressive stress of any significant magnitude. Delamination should not occur for these laminates according to the analysis.

The stress-strain curves which were determined from experimental data for the Type I laminates were similar to those which were predicted by the laminate analysis.

3. Uniaxial Stress-Strain Data for Type I Specimens

During the quasi-static tension tests, outputs from the Instron load cell and the strain gage bridge amplifiers were recorded as functions of time on strip chart recorders. The load and axial strain data were tabulated and the axial stress-strain curves plotted as shown in Fig. 9. Some specimens were instrumented with small strain gages at the edge of the specimen which were oriented transversely to the load direction. These gages measured the local strains in the vicinity of the free edge of the specimen. Although this method of data acquisition, as contrasted with direct plotting of the

17

stress-strain curve, requires an additional data reduction step, it does provide a plot of load and strain relaxation during the periods when the crosshead of the screw-type machine is stopped for microscopic observations of damage.

As described in a previous section, real-time ultrasonic attenuation values were taken for Type I specimens using the DPO system described earlier. In all cases but one, the attenuation was observed to rise suddenly in the neighborhood of the knee. Because of the relative discontinuity in data points this data is not shown here in graphical form.

The stress strain curves shown in Fig. 9 are typical for Type IA and Type IB material. Although the IA material had an initial curvature, the average strength and average initial elastic modulus were greater than the corresponding average values for Type IB material. These values are shown in Table II. The strain to failure of both materials was essentially the same. Stress-strain curves for both materials exhibited a distinct "knee" but the percent change in stiffness at the knee was not a characteristic of either material. The bi-linearity in the tensile response is evidenced in the strain gage output from both axial and transverse gages by a knee in the strain-time curves.

Comparison between the stress-strain data and at-load microscopic observations shows that the knee in the stress strain curve occurs above the stress level where the transverse cracks in the 90° plies are first observed. In fact, the discrepancy is quite large. The knee has occurred around 2000 lb. load (37 ksi) for most of our data. The lowest recorded value is 1750 lb. (32.5 ksi). Cracking is observed by light microscope observations of the specimen edge at loads as low as 1000 lb. and by 1500-1800 lb. the cracking is usually well developed, especially in Type I material.

18

Neither the knee in the stress-strain curve nor the first observation of
a transverse crack through the microscope should be construed as an
indicator of first ply failure initiation. The knee in the stress-strain
curve results when a transverse crack grows to sufficient size, or the
density of transverse cracks increases sufficiently, to increase the
compliance of the specimen and alter the local strain field at the location
of a strain gage some distance from the crack. Since the specimen edge is
scanned microscopically after a finite increment in load from a previous
observation, the crack could have initiated during that loading increment
or even have been too small to be detected during a previous scan. It is
also possible that the first ply failure could go undetected if it were
to occur on the edge of the specimen not being scanned.

4. Damage Observations for Type I Specimens

Some details of the damage development are shown in Fig. 10. The
photographs were made through a microscope during loading of a Type I
laminate. At a stress level of 25 ksi or so the 90^0 cracks begin to form
as shown in Fig. 10a. The crack usually begins in one of the 90^0 plies and
quickly spreads across into the other one. As the load increases the crack
opens up. Although we cannot say that these cracks never extend across the
width, we have never observed a crack on the opposite edge at a position
which would be directly opposed to an observed crack. Hence, we postulate
that the crack also grows across the specimen width as the load is increased.
The spacing of the cracks also changes, i.e, new cracks develop during con-
tinuing increase of load. This initiation process appears to continue up to
applied stress levels of 50 ksi or so at which time the spacing (and density
or number) of cracks appears to stabilize. At approximately that level

19

delamination is observed. In some cases we have noticed that delamination
is nucleated by the extension of the transverse cracks in the 90° ply into
the 90°-45° ply interface as shown in Fig. 10c. Delamination quickly seeks
the midplane of the specimen and grows as shown in Fig. 10d. Final fracture
is not coincident with delamination and the separation of the de-
laminated edges may reach approximately half a ply thickness in magnitude.
The delamination process frequently begins in the neighborhood of the region
below the ends of the tabs and spreads essentially along the entire length
of the specimen quite rapidly.

A summary schematic of the damage sequence in Type I specimens is
shown in Fig. 11. Damage initiation occurs first in the 90° plies in a
plane transverse to the load axis, as predicted by the laminate analysis.
Our microscope observations are never able to resolve the actual initiation
event since we do not know where to look for those events until they occur.
Hence, our earliest observations will always occur at loads beyond those
predicted as can be seen from the discussion above. Further nucleation
of cracks occurs over a range of increased load until a stable spacing of
cracks develops as shown in Fig. 10b. That spacing is usually one and
a half to two times the specimen thickness. The cracks grow through the
(90° ply) thickness and, apparently, across the specimen width. At about
two thirds of the ultimate strength, the transverse cracks grow into the
90°-45° ply interface where they frequently branch, and subsequently spread
along that interface in a longitudinal plane (parallel to the load axis)
thereby nucleating delamination. Failure occurs by a transverse fracture
of the 0° plies which is quite distinct in nature. It has not been
established that final fracture coincides with the position of a transverse
crack in the 90° plies but that association is suggested by the fracture

20

mode and suspected by the investigators.

5. Uniaxial Stress-Strain and Attenuation Data for Type II Specimens

The behavior of the Type II specimens is substantially different from the Type I laminates. The experimental procedures used in testing these specimens were the same as those presented earlier for Type I material. Ultrasonic attenuation values were recorded in real-time during loading using the Matec automatic recorder. A typical stress-strain curve for a Type II specimen is shown in Fig. 12. Although there are some differences between the average strengths of the several laminate types (Table II), a more apparent and important difference in response is the much less pronounced knee in the Type II stress-strain curve. The change in stiffness associated with the knee is on the order of 6% in Type II laminates compared to approximately 18% in Type I specimens. As is the case for the Type I material, the knee in the Type II stress-strain curve corresponds to a stress level higher than that where transverse cracks in the 90° layers were first observed. However, as will be discussed later, the transverse cracks in Type II specimens are generally shorter and delamination was not observed in the gage section of the specimen.

The real-time attenuation data taken by the automatic recorder during the testing of the Type II specimens was similar to that observed for Type I. In all cases tested, the Type II specimens displayed a sudden rise in attenuation at the knee of the load-strain curve (Figs. 13 and 14). In Fig. 15 our estimate of the knee in the load-strain curve is indicated by the vertical dotted line. It is apparent that some damage process occurs in the volume of the specimen immediately under the transducer at and above the knee of the load-strain curve.

As noted earlier, in order to make visual microscopic examinations along

21

the edge of the specimens, crosshead motion was stopped and held fixed for a few minutes. During these test sequences, the automatic attenuation recorder was allowed to continue running. The results of these tests are shown in Figs. 15 and 16. At constant displacement, the load was observed to decrease. During this time, the attenuation was observed to increase, indicating the continuing growth of damage at constant displacement. This was especially true for specimen 265*3 in Fig. 16, where the increase in attenuation with decreasing load at constant displacement is indicated by those regions in the attenuation-load curves having apparent multiple-values of α for the same load. It should be noted that the attenuation curves shown earlier in Figs. 13 and 14 are the same respective curves given in Figs. 15 and 16. In the earlier figures, the changes in attenuation at constant displacement were removed from the curves to show the overall behavior of the attenuation for continuously increasing load.

6. Damage Observations in Type II Specimens

Damage development in these laminates is evidently affected by the ply sequence in several ways. Because the 90° plies are not adjacent to one another, the size of the transverse cracks that develop in these specimens is smaller, at least in the z direction. It would seem that the situation at the tip of those cracks (at the interfaces with the adjacent plies) should be less severe than for the Type I laminate where the cracks are twice as long in the z direction. If final failure is nucleated by these cracks, it would be reasonable to expect somewhat greater strength from the Type II laminate. No such consistent trend could be discerned in the data, and both laminates fail below the predicted strengths. Small variations in the manufacturing can easily produce differences of this magnitude so no final conclusions about this

22

can be established. There is also some indication that the stable spacing of 90° ply cracks is smaller for the Type II laminates.

Of course, the largest difference in the two layups is the σ_z stress distribution. Delamination should not occur in Type II laminates, and none is observed in the center sections of the specimen. However, as shown in Fig. 17, delamination is induced by the tabs as they tend to peel up just outside of the grip area due to unresolved moments on the tab section. That delamination is generally confined to the grip area, spreading into the grips and towards the gage section, typically over lengths of one half inch or so. The final fracture is even more distinctly transverse than the Type I laminates.

Several additional comments concerning the nature of damage development can be made. Cyclic loading appears to influence the growth stage of damage development. The nature of the resulting damage does not appear to differ significantly from static loading, but the degree of damage does. Damage growth has also been observed when no additional load is applied with hold-times of a few minutes at loads near the ultimate strength of the laminates. In one case, a Type I specimen failed approximately ten seconds after the cross-head of a screw-type loading frame had been stopped for observation. In that case, cracks in the 90° plies were seen to spread into the interface with 45° layers, branch, and grow just prior to failure. Finally, the reproducilbility, and, therefore, the predictability of these laminates appears to be reasonably good for composite materials. We have not investigated a large number of specimens so that exact coefficients of variation, etc., are not available, but behavior from specimen to specimen is sufficiently consistent in most cases to allow systematic experimental investigation of a basic type without the need for statistically significant numbers of tests at every point on the learning curve.

23

SECTION IV

CONCLUSIONS

Based on our observations, outlined above, the following preliminary observations and conclusions are drawn.

1. It appears that initiation, growth, and final fracture stages are identifiable during static and cylic loading. Initiation occurs in the 90° plies with cracks which appear early in the load history, with crack faces essentially perpendicular to the load axis. The cracks grow by spreading through the layer thickness (or thicknesses for adjacent 90° layers), then, apparently, across the specimen width, and into ply interfaces in some instances. Cracks in the 90° layers have also been observed to branch into adjacent 45° layers rather than spread along the (axial) 90°-45° interface. Fracture is initiated when combined damage causes failure of the 0° plies.

2. Cyclic loading appears to cause additional flaw growth compared to static loading to an identical load level. However, the basic nature of the damage appears to be unchanged. Flaw growth, specifically, growth of the transverse cracks in the 90° plies, has been observed at -load (actually at constant cross-head position) with corresponding relaxation of the load. In one case failure of a specimen occurred while the test was stopped at a load quite near the expected ultimate strength level.

3. The single most salient divergence from laminate theory predictions is that damage stages have less than absolutely separate distinguishing features. Crack formation and growth in the 90° laminae, for example, occurs over a large range of loads, and the spacing of the cracks becomes gradually smaller until what appears to be a stable spacing is reached. This continuous sequence of events in reality corresponds to the discrete knee in the stress-strain curve predicted by (idealized) laminate failure theory.

24

4. Relatively little of the total potential of combined experimental and analytical investigation has yet been realized. The exact nature of damage development in these materials has not yet been established. It remains to be seen how the initial flaws actually do grow and combine to cause failure. The change in response as damage develops under various loading histories is also incompletely characterized. Realistic models of material response during damage development are yet to be formulated.

The need for further work is apparent. With the help of a variety of experimental techniques, some still under development in our laboratories, further attempts to establish improved understandings of these phenomena will be made and representations will be attempted.

REFERENCES

1. Wu, E. M., "Strength and Fracture of Composites", in _Composite Materials_, Vol. 5, Academic Press, 1974.

2. Smith, C. W., "Limitations of Fracture Mechanics as Applied to Composites", in _Anelastic Behavior of Composites_, ASME, Proc. of Winter Meeting, Houston, Texas, Dec., 1975.

3. Rosen, R. W. and Zweben, C. H., "Tensile Failure Criteria for Fiber Composite Materials", NASA-CR-2054, 1972.

4. Kulkarni, S. V. and Rosen, B. W., "Design Data for Composite Structure Safe Life Prediction Analysis Evaluation", AFML-TR-73-225, Chap. 5.

5. Halpin, J. C., Waddoups, M. E., and Johnson, T. A., "Kinetic Fracture Models and Structural Reliability", Int. J. of Fracture Mechanics, Vol. 8, (1972), pp. 465-468.

6. Eisenmann, J. R., Kaminski, B. E., Reed, K. L., Wilkens, D. J., "Toward Reliable Composites: An Examination of Design Methodology," J. Comp. Matls., Vol. 7, (1973) pp. 298-308.

7. Hahn, H. T. and Pagano, N. J., "Curing Stresses in Composite Laminates", J. Composite Materials, Vol. 9 (Jan. 1975), p. 91.

8. Pagano, N. J. and Pipes, R. B., "Some Observations on the Interlaminar Strength of Composite Laminates," Int. J. Mech. Sci., Vol. 15 (1973) pp. 679-688.

APPENDIX A

For a stress free temperature which differs from room temperature the midplane strains are given by

$$[\varepsilon^0] = [A]^{-1}[N + N^T] \qquad (a)$$

where $[\varepsilon]$ is the matrix of midplane strains, $[A]^{-1}$ is the inverse of the plate stiffness matrix in the absence of bending, $[N]$ is the column matrix of applied in-plane resultants, and $[N^T]$ is the ambient temperature resultants due to thermal residual stresses given by

$$[N^T] = \int [\bar{Q}][\alpha]\Delta T dz \qquad (b)$$

where $[\alpha]$ are the thermal expansion coefficients, listed in Table III. The stresses in a given layer are then

$$[\sigma]^k = [\bar{Q}]^k[[\varepsilon^0] - [\alpha]\Delta T]^k \qquad (c)$$

The pertinent maximum strain condition is,

$$\sigma_x^{90^0} \leq \frac{Y}{\sin^2\theta - \nu_{21}\cos^2\theta} \qquad (d)$$

where Y is the tensile failure stress in a direction perpendicular to the fiber direction, and θ is the direction of the fibers relative to the load axis, "X".

For a stress-free temperature of 278^0F and the material properties described in Table III, condition (d) yields,

$$\sigma_x^{90^\circ} \leq 8,200 \text{ psi}$$

or,

27

N_x = applied load for one inch wide specimens

N_x = 950 lb.

which corresponds to an applied stress of 1750 psi. If the strength is 10 ksi instead of 8.2, N_x is 1400 lb. and the applied stress prediction for 90° ply failure is 26 ksi.
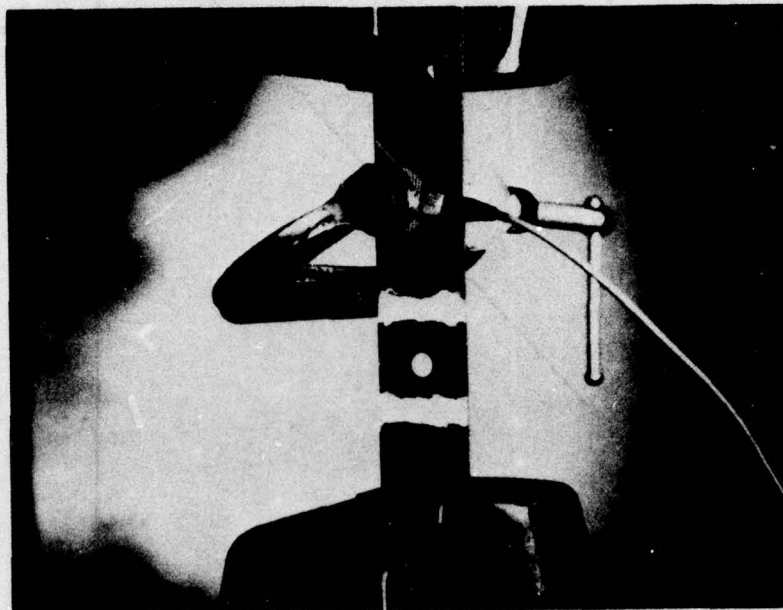
Figure 1 Ultrasonic transducer clamped to a composite specimen mounted in testing grips.
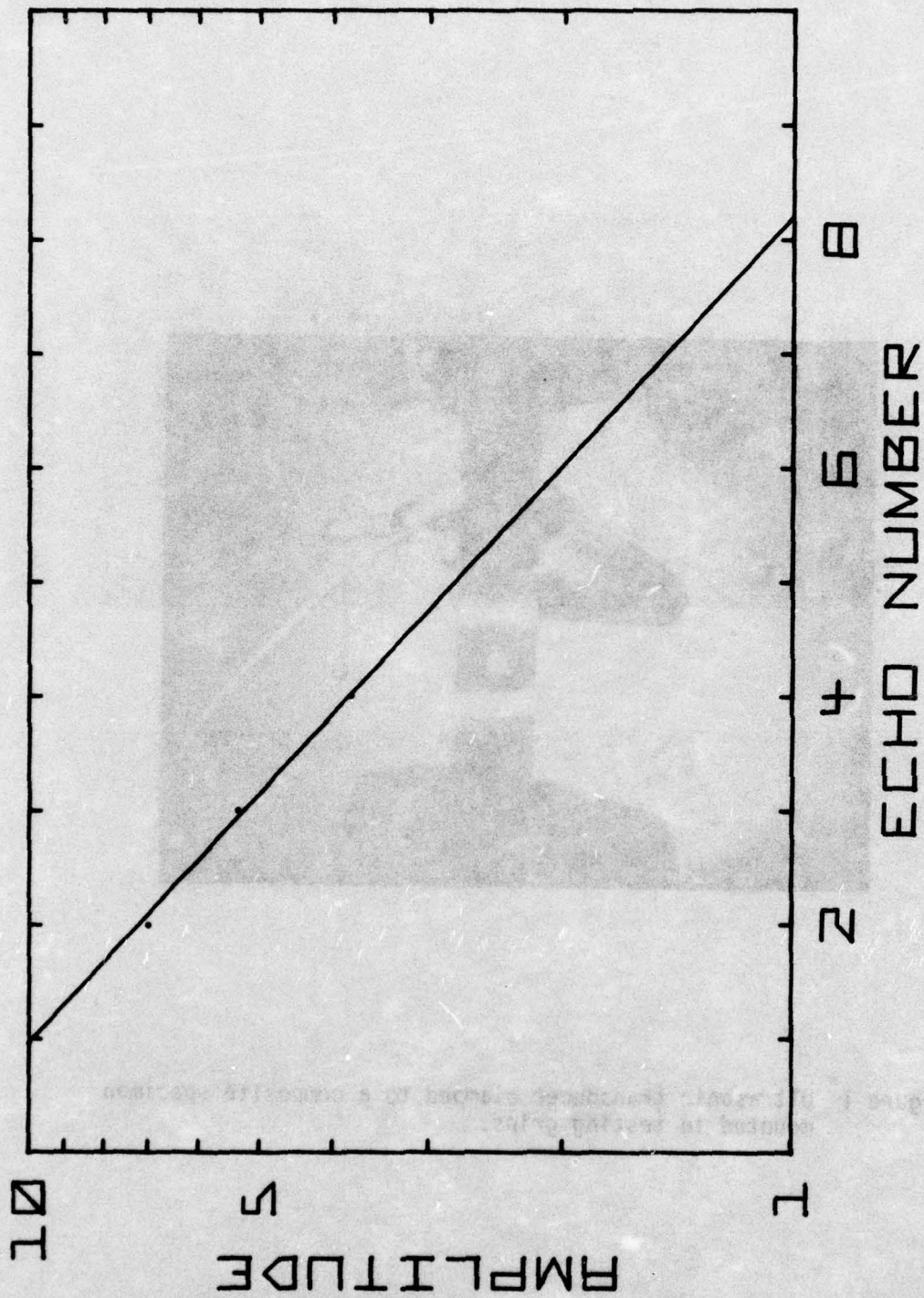
Figure 2 Ultrasonic attenuation plot generated by digital processing oscilloscope.
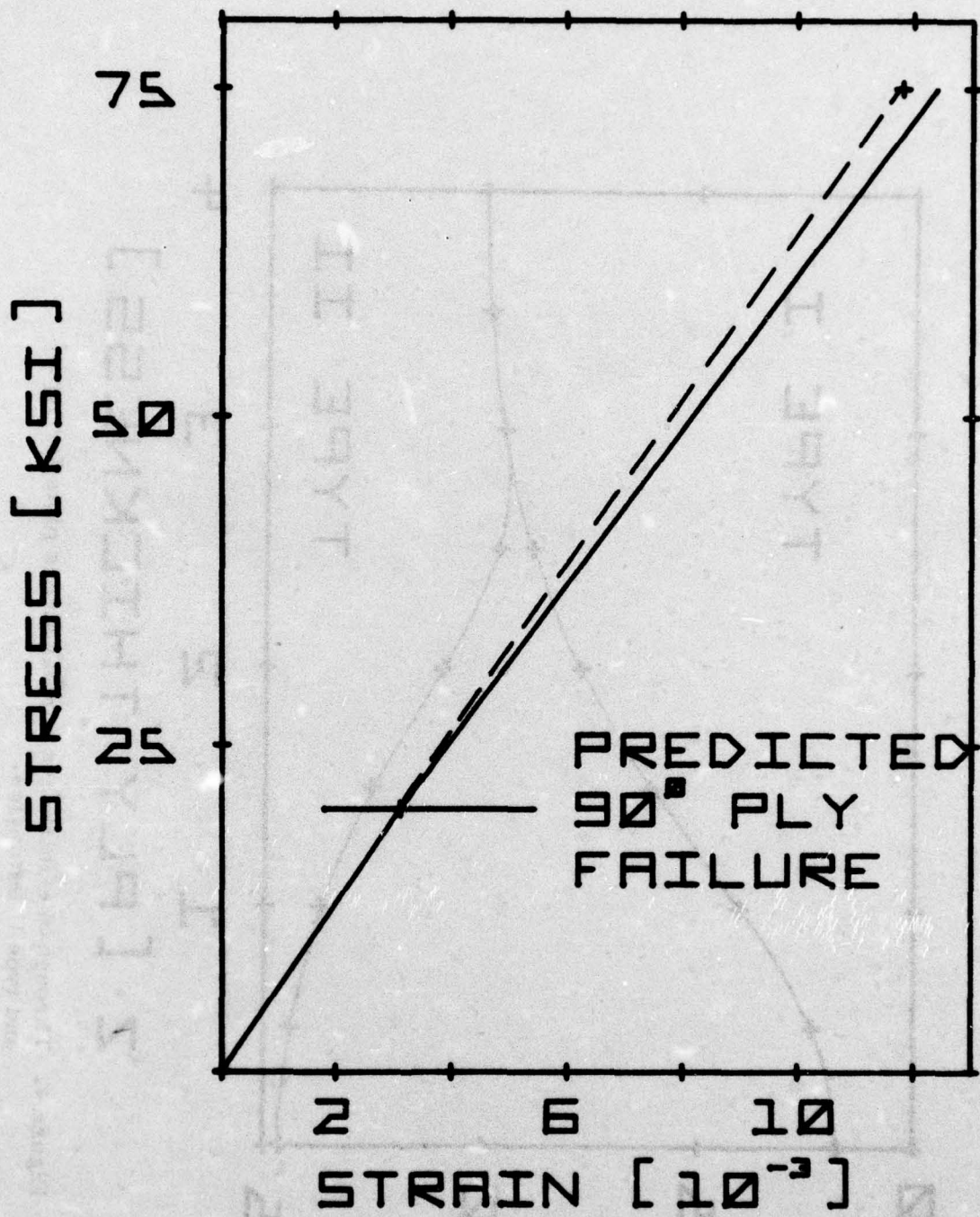
Figure 3 Stress-strain response predicted by laminate theory.

31
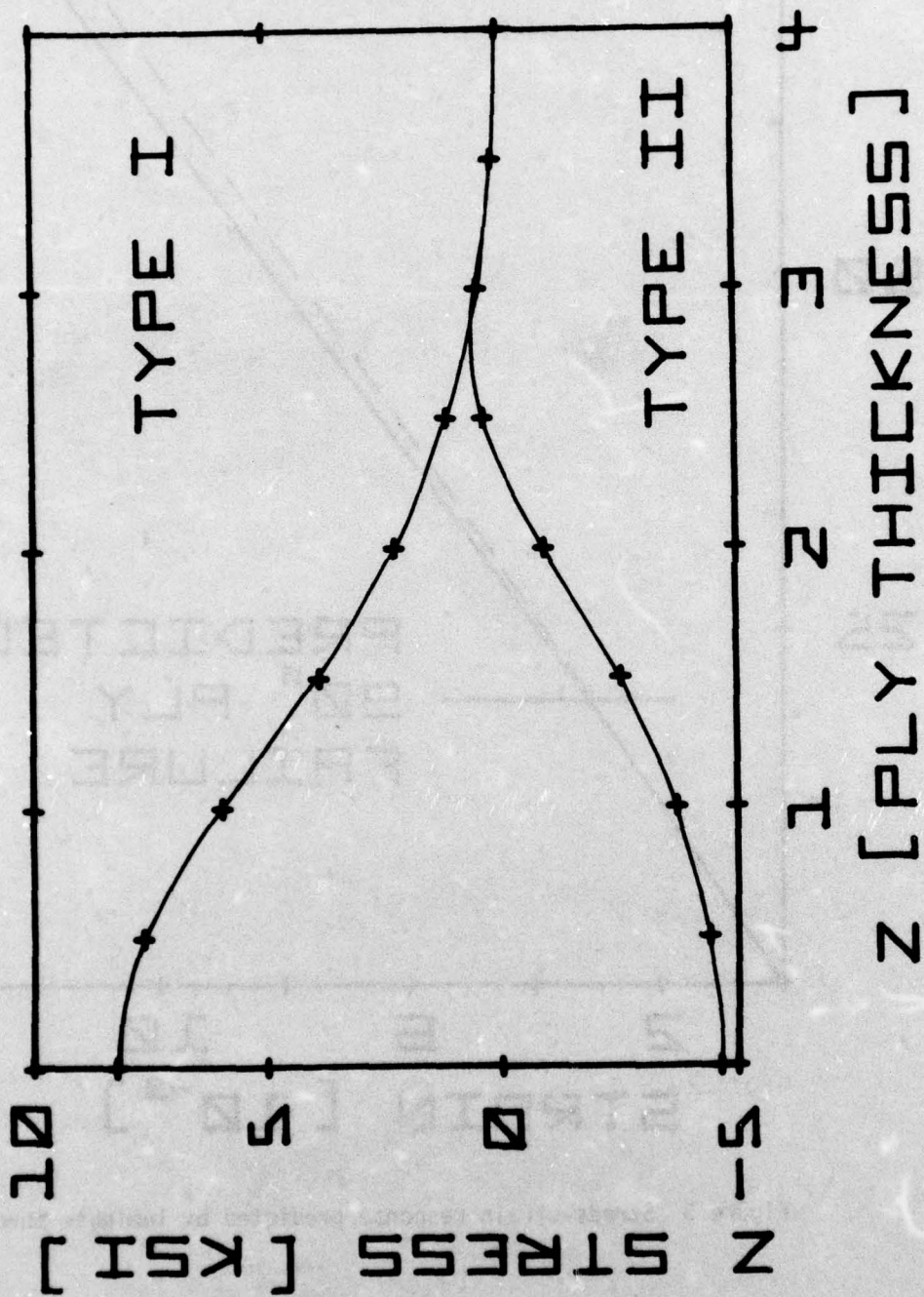
Figure 4. Through-the-thickness normal stress plots for type I and type II laminates.
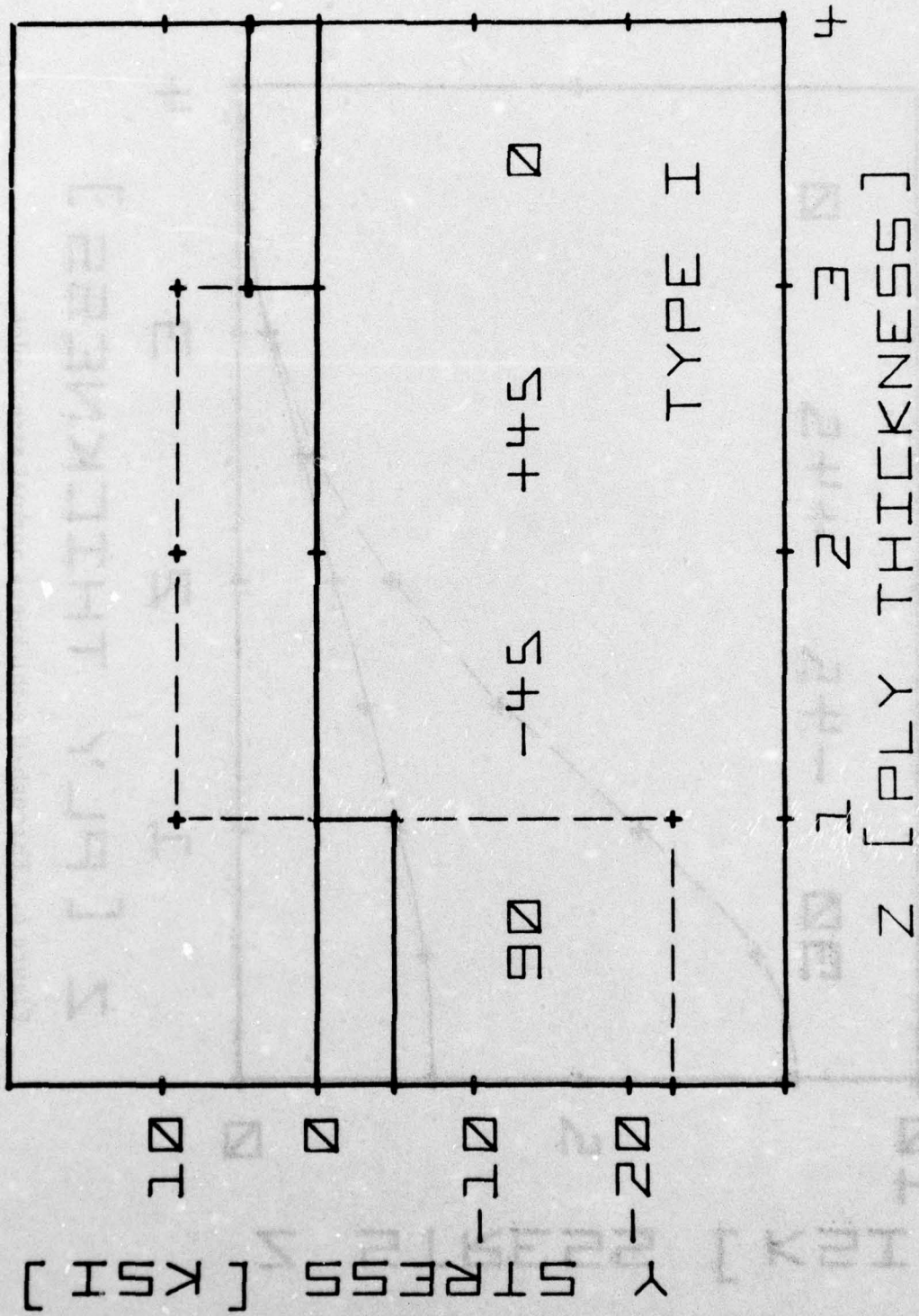
Figure 5. Transverse in-plane normal stress plot for a type I laminate.
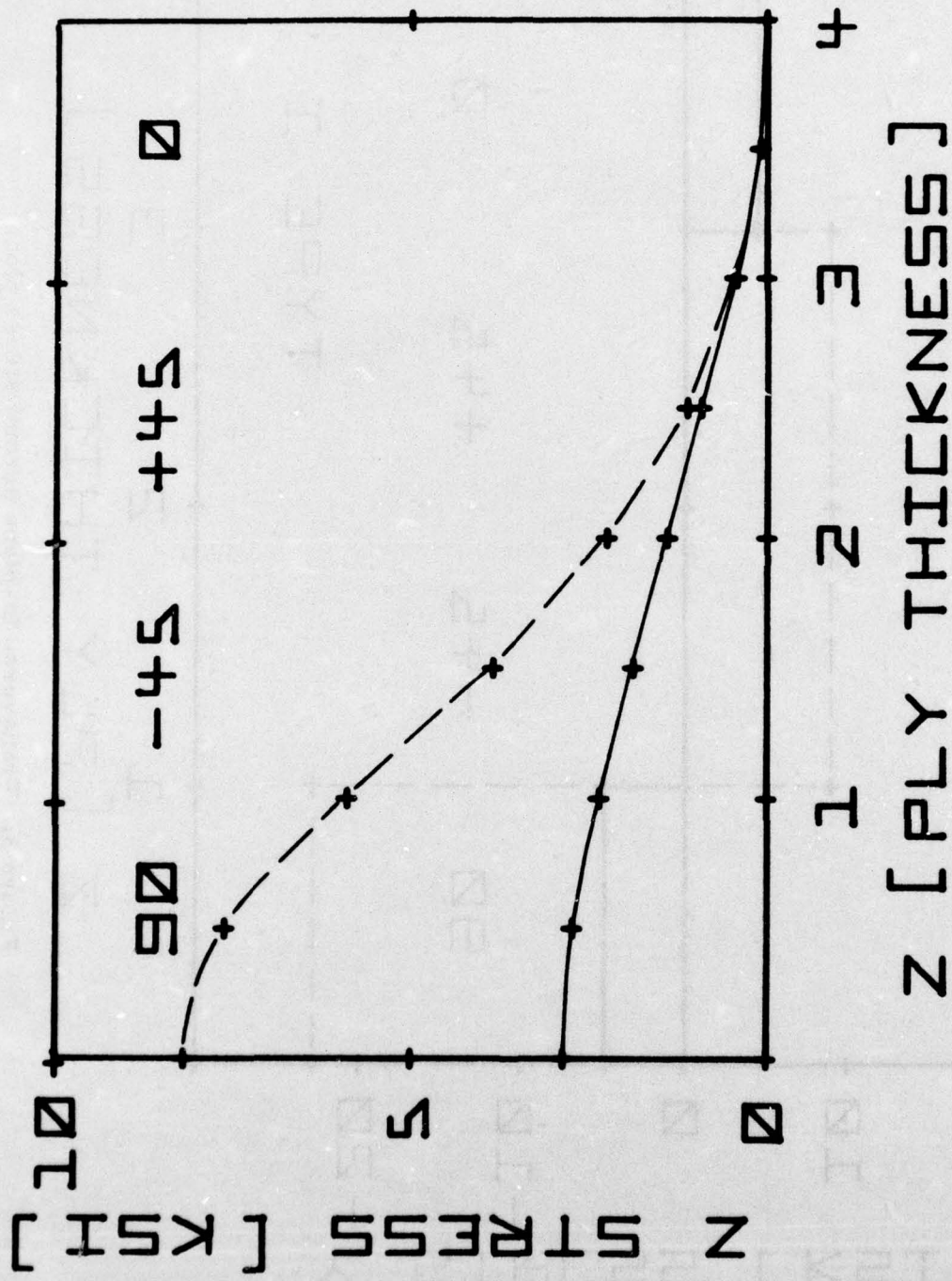
Figure 6. Through-the-thickness normal stress plot for a type I laminate.

34
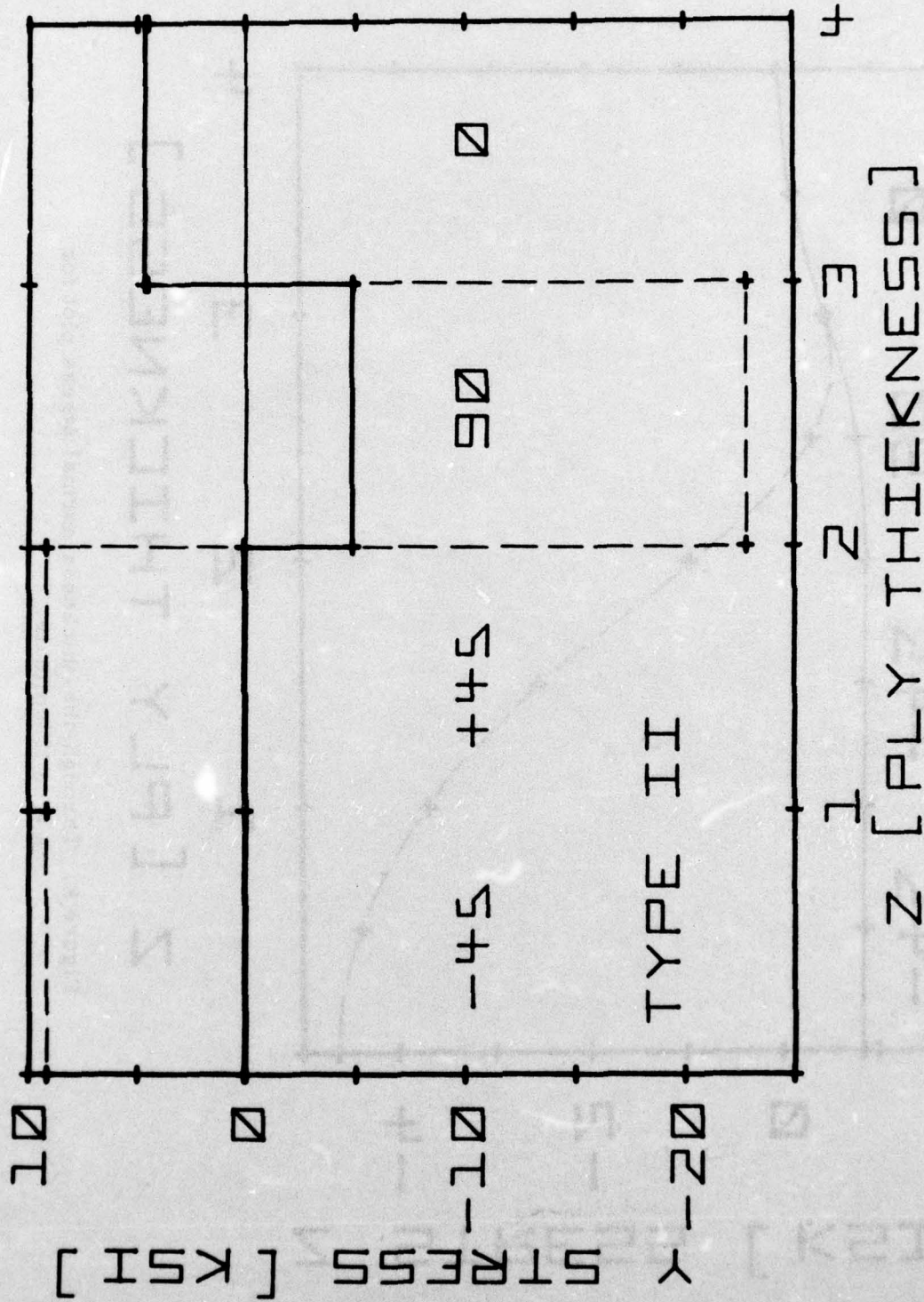
Figure 7. Transverse in-plane normal stress plot for a type II laminate.
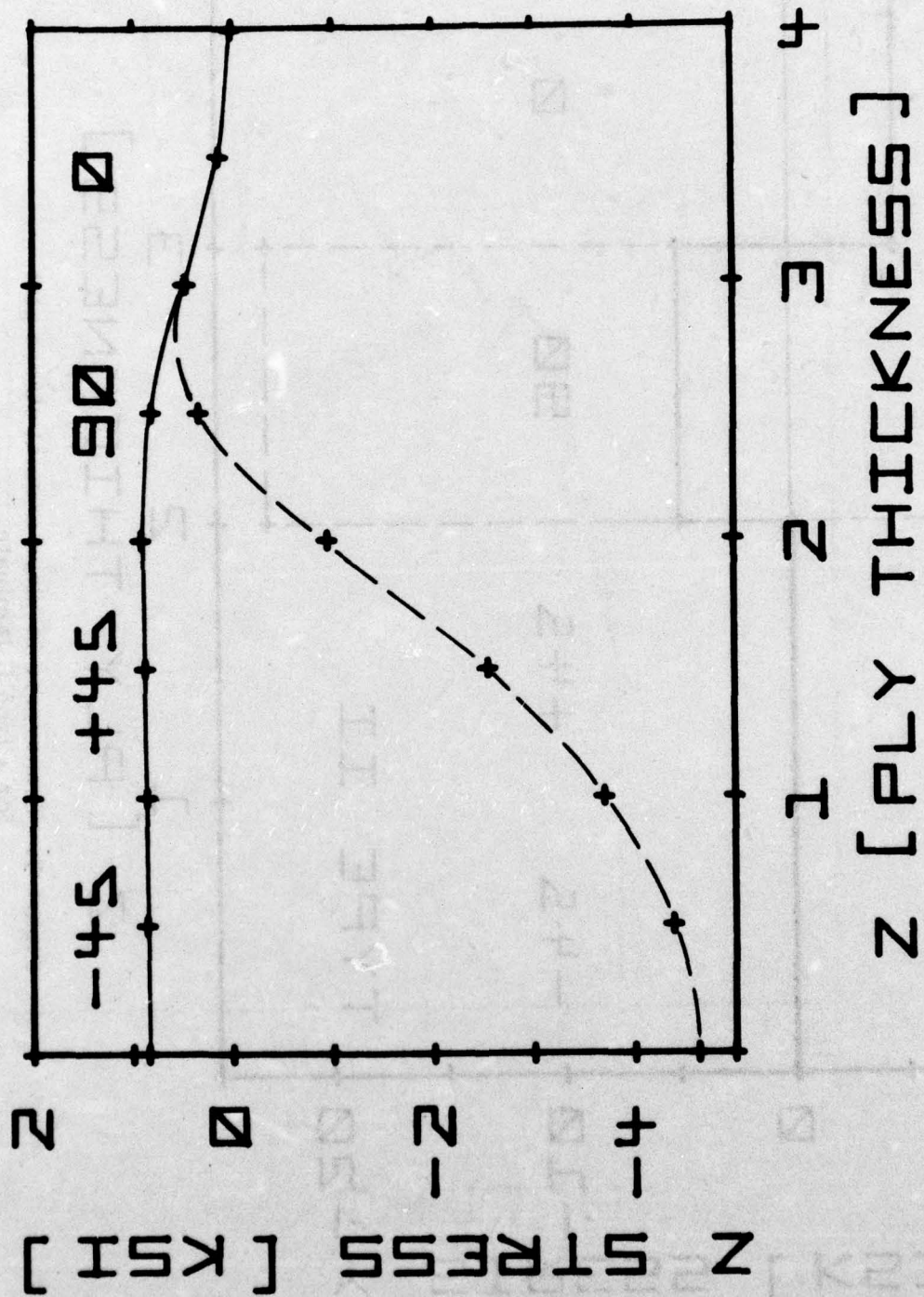
Figure 8. Through-the-thickness normal stress plot for a type II laminate.
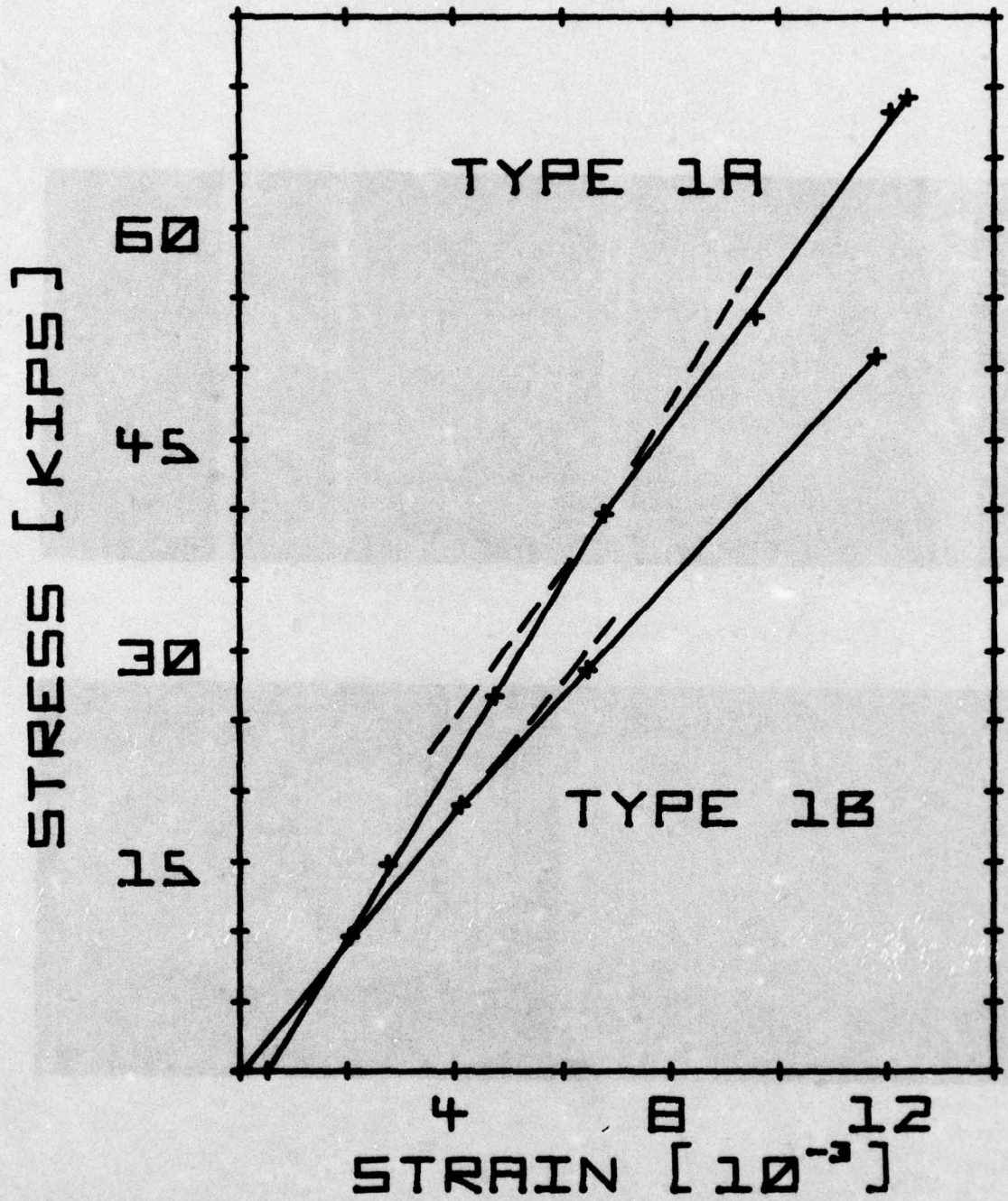
Figure 9 Typical experimental stress-strain data for type I laminates.
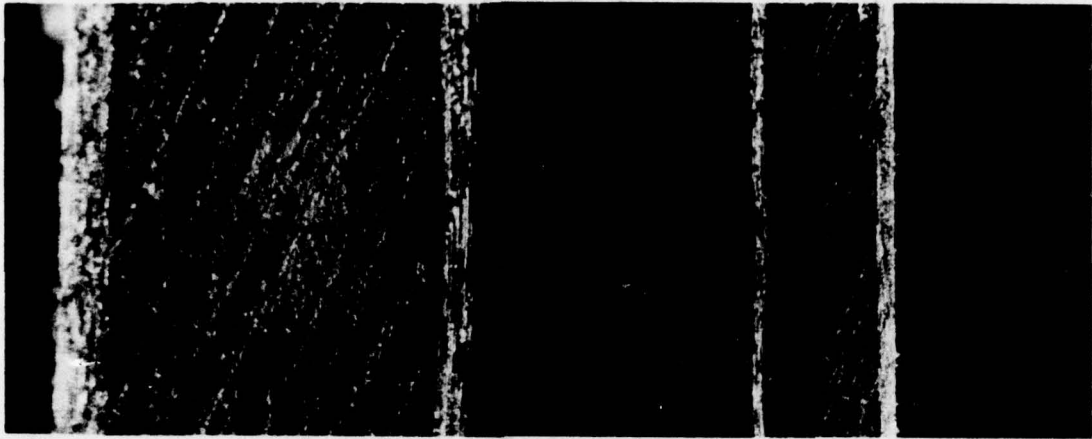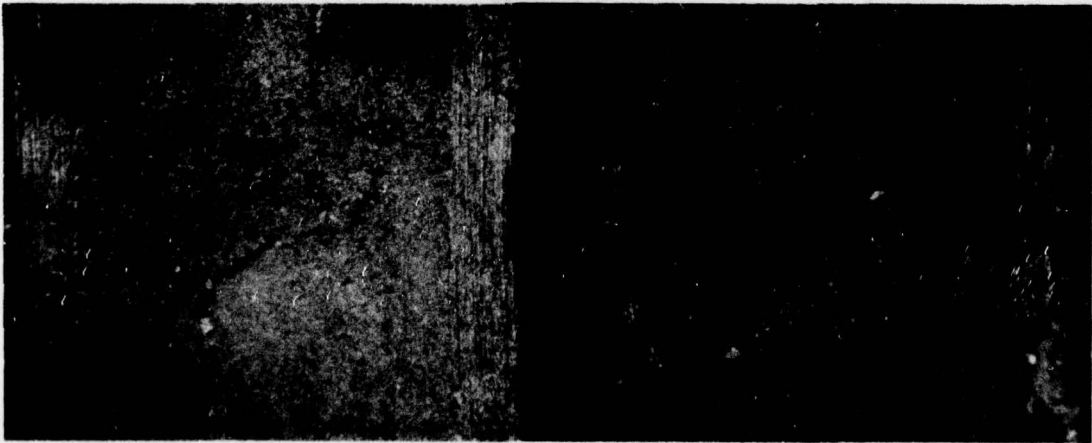
Fig. 10 Microscope photographs of transverse cracking and development of delamination in type I laminates. (a,c,d at 30X, b at 10X)
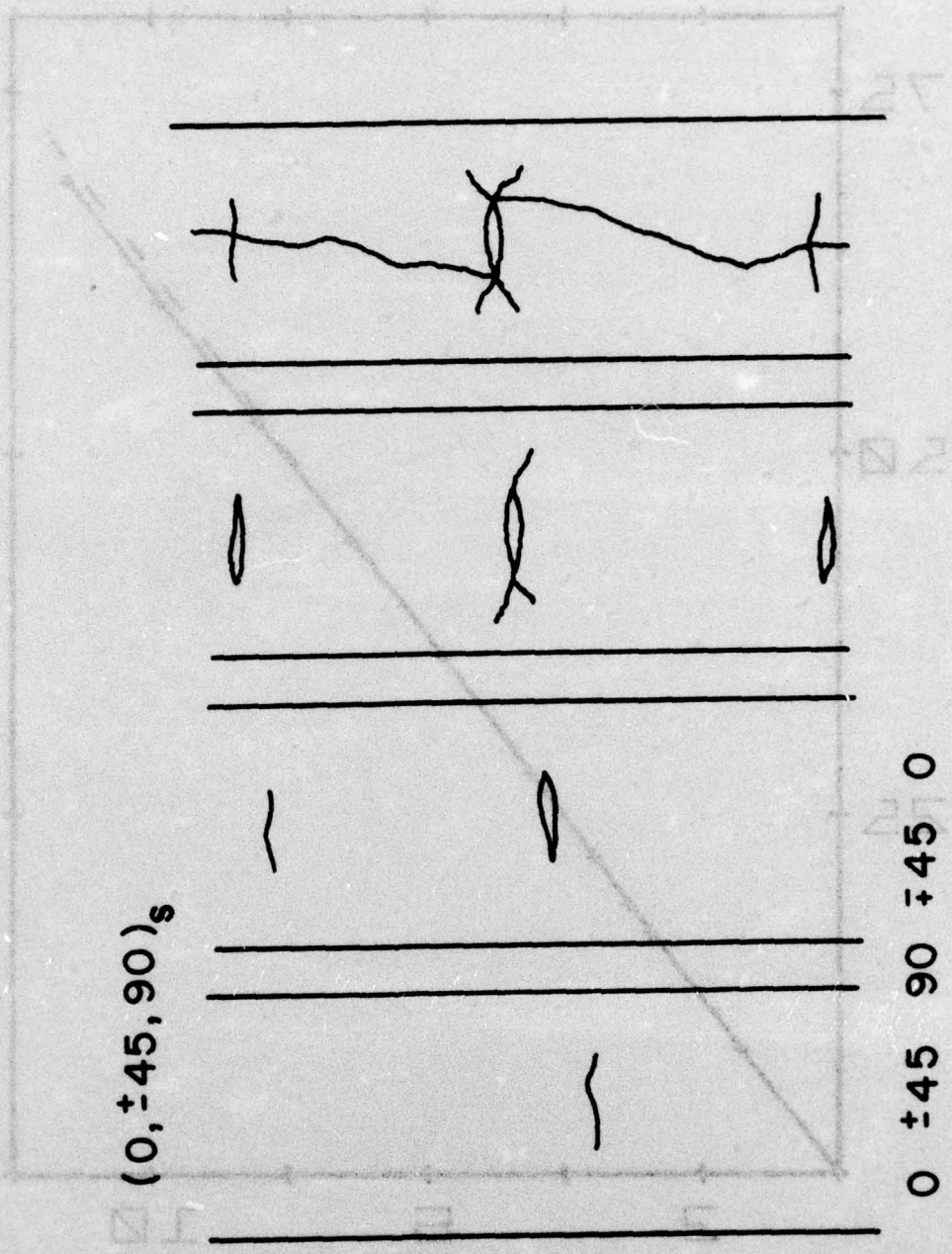
Figure 11 Schematic diagram of damage development in type I laminates.
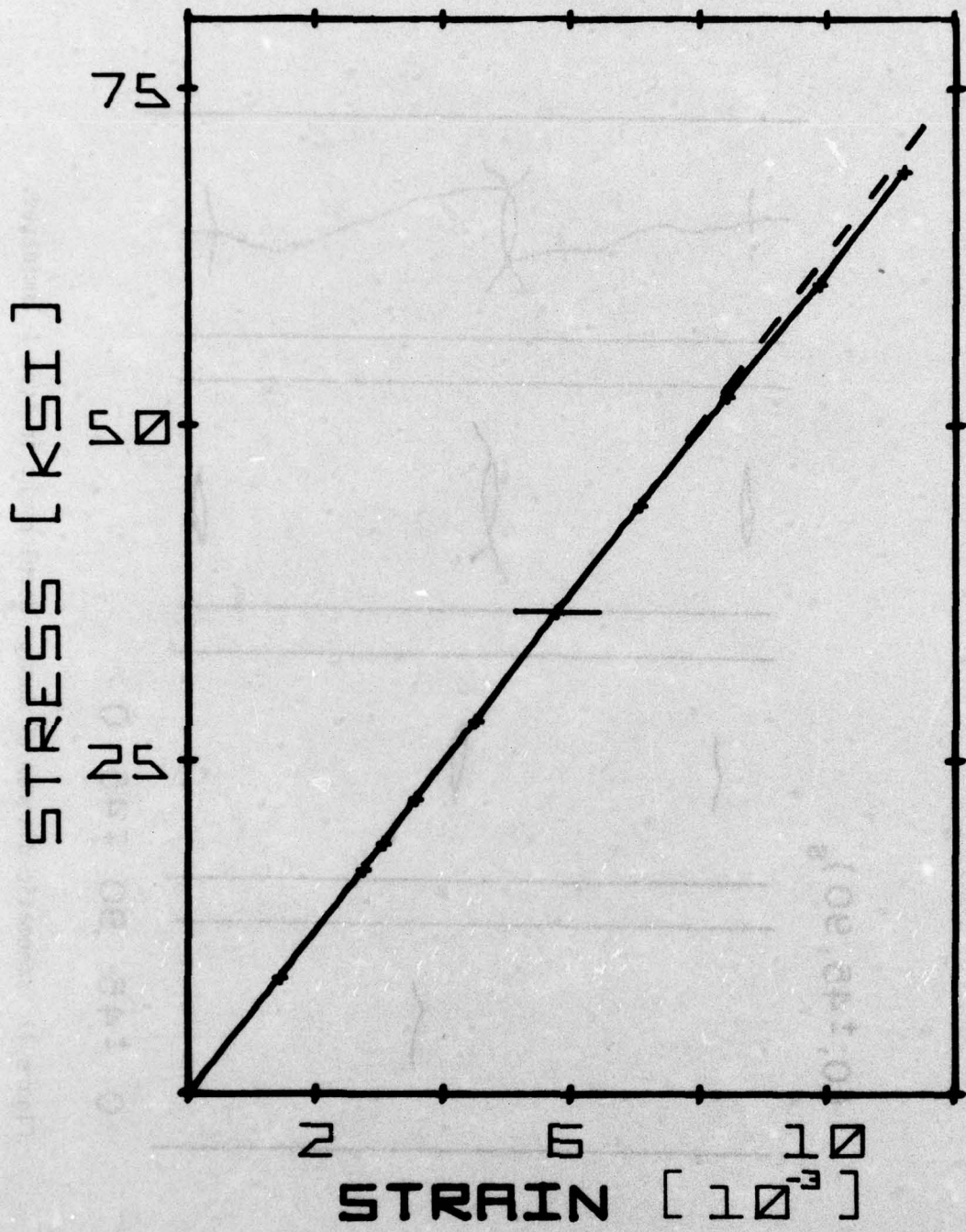
Figure 12 Typical experimental stress-strain data for type II laminates.

40
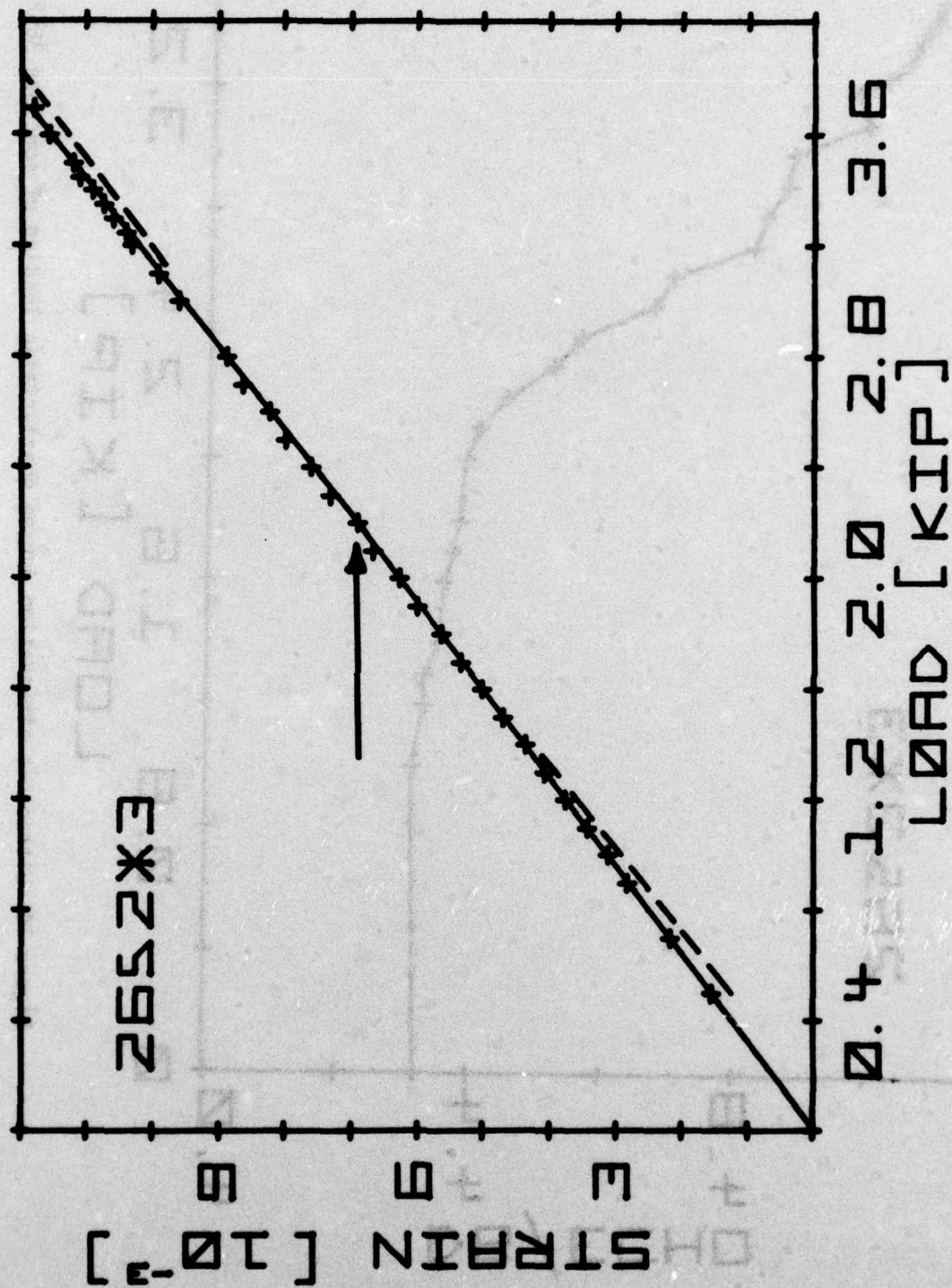
Figure 13 Stress-strain data for specimen 2652*3, a type II laminate.
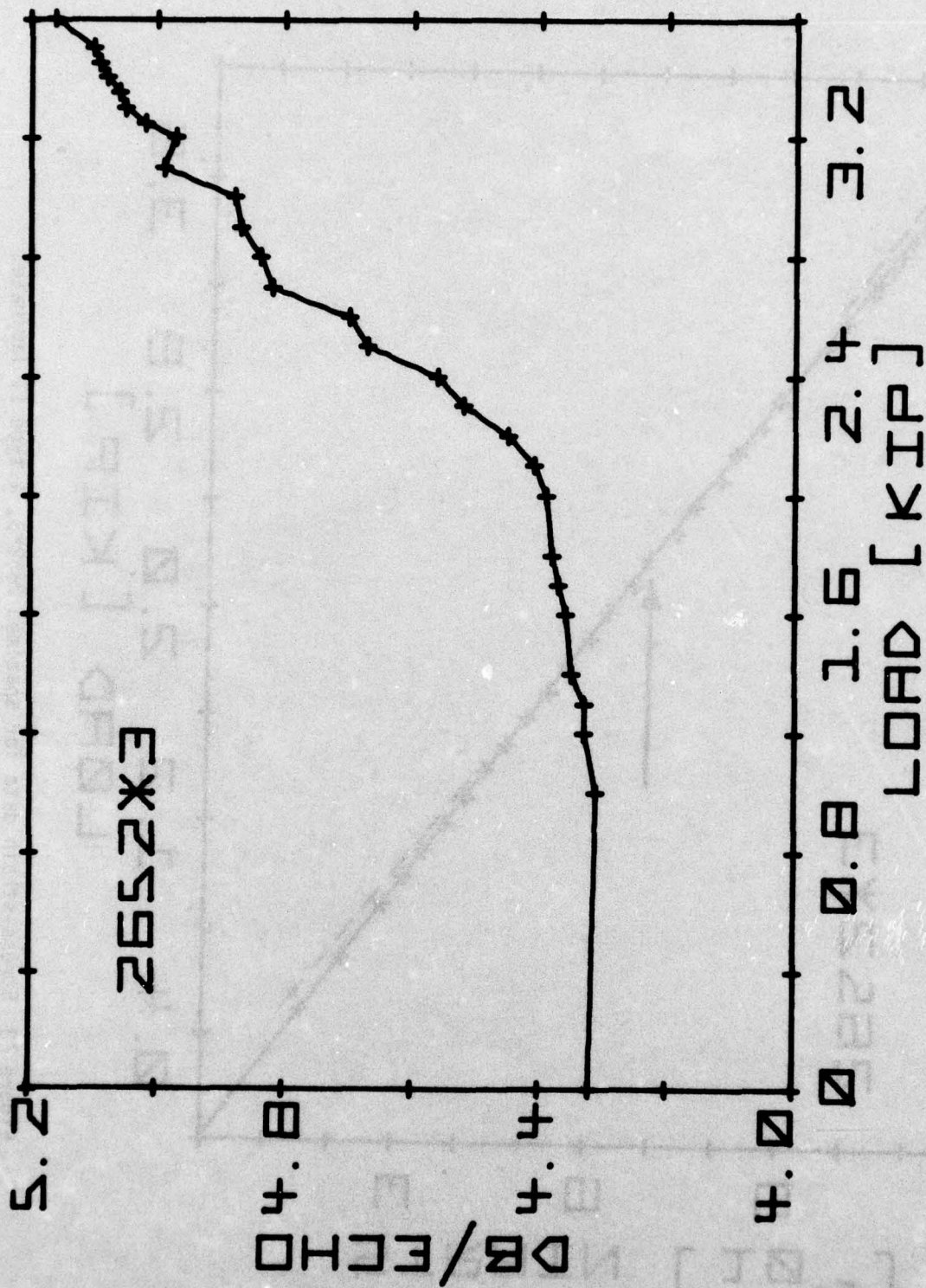
Figure 14 Ultrasonic attenuation during quasi-static loading of specimen 2652*3.
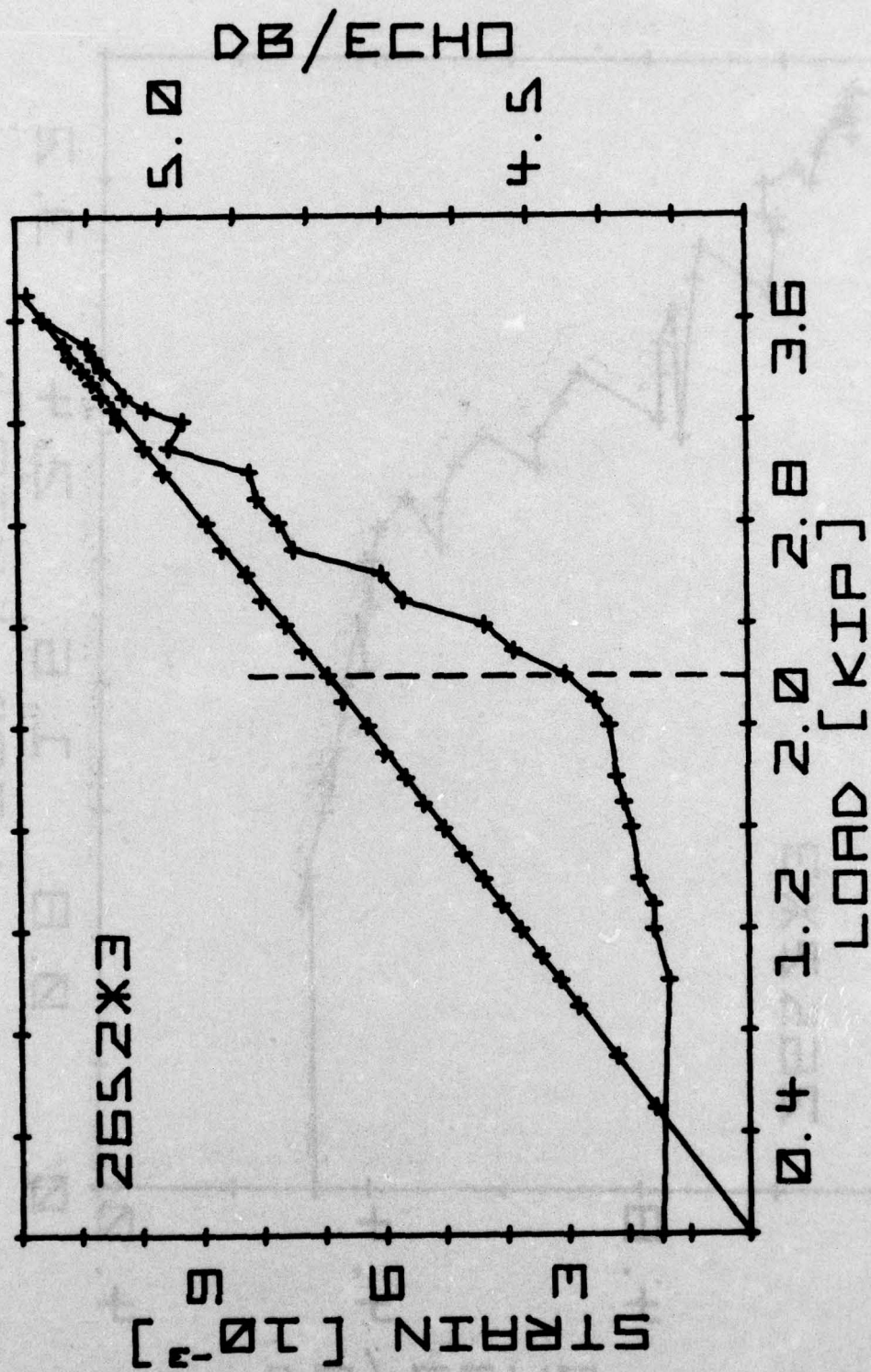
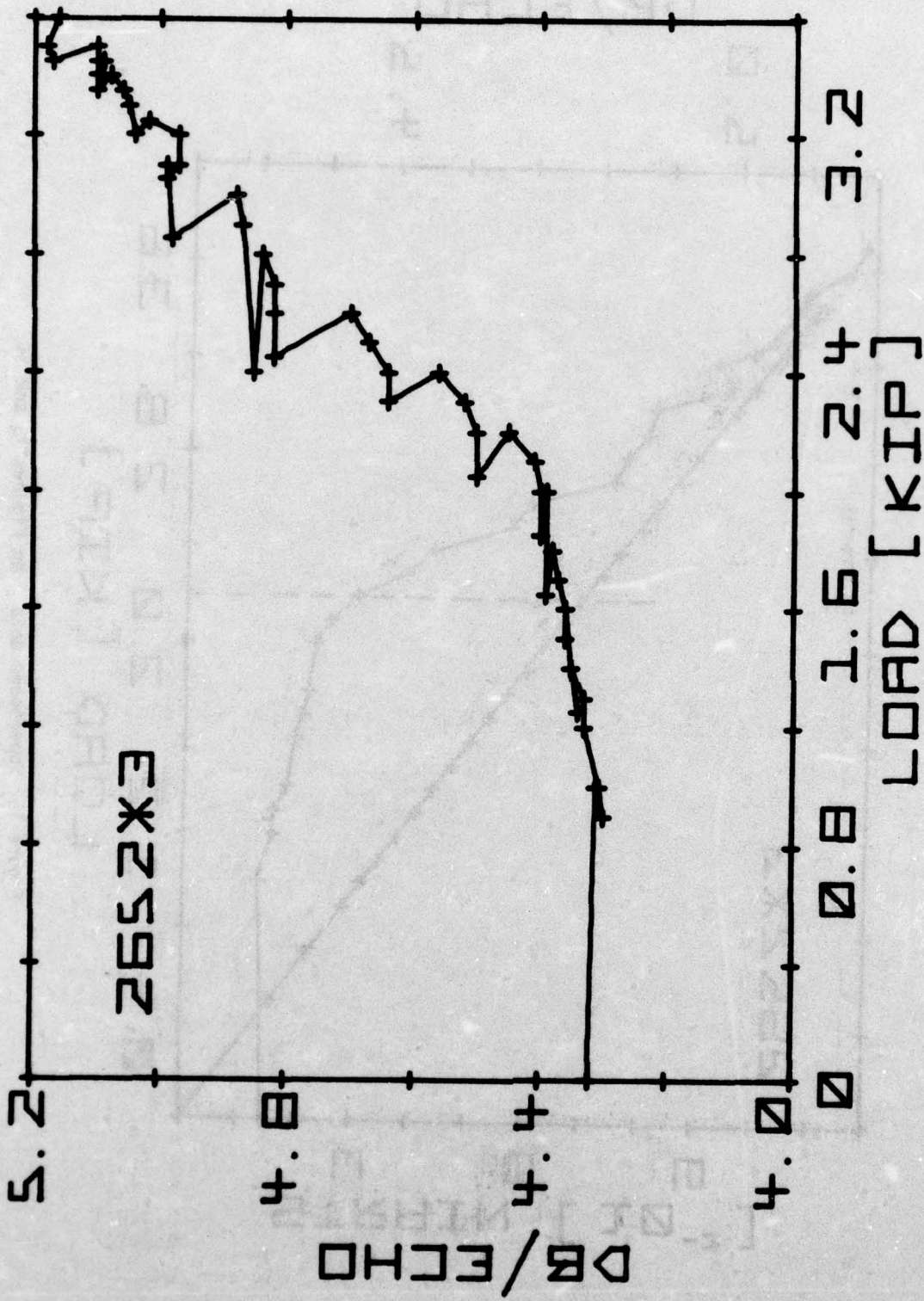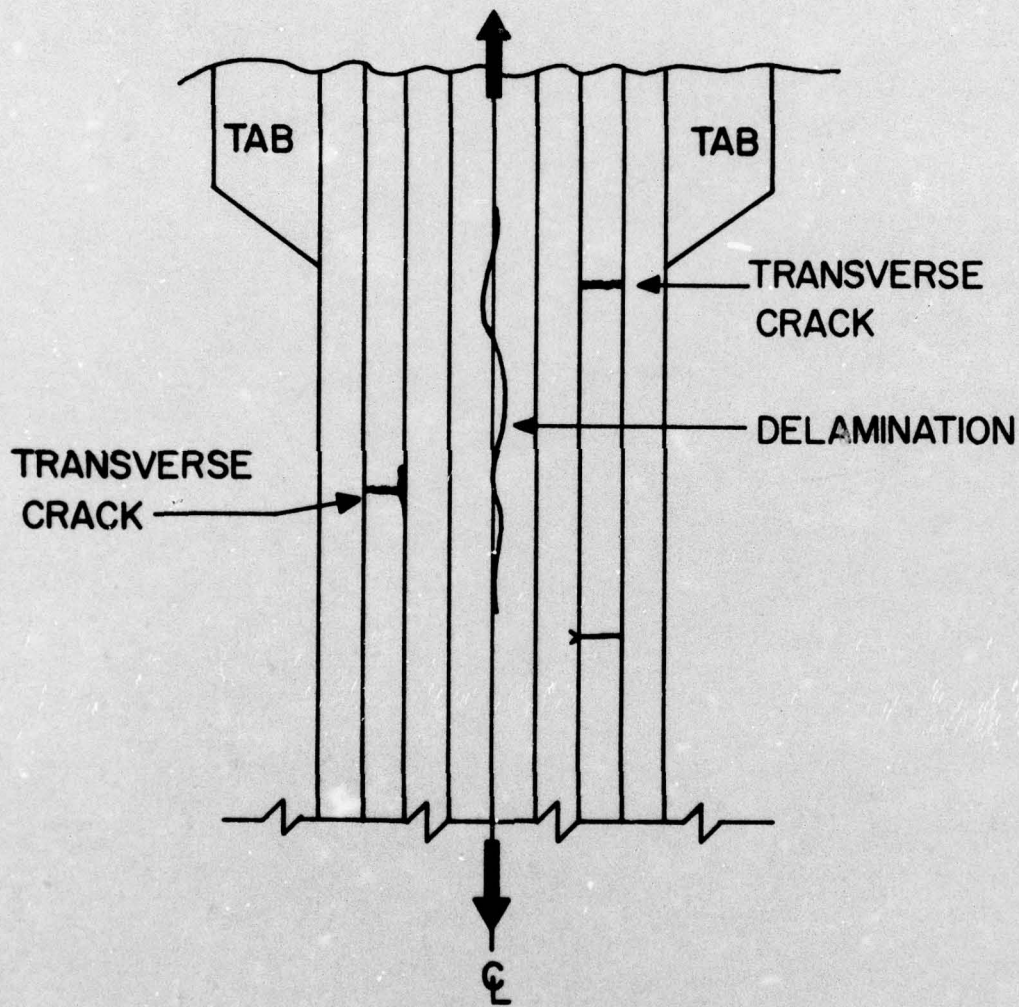Figure 15 Superposed data from Figures 13 and 14.

Figure 16 Effect of pauses in cross-head motion on ultrasonic attenuation data.

AS 3501 G/Ep
SPECIMEN TYPE II
(0°, 90° , +45°, -45°)s

Figure 17 Schematic diagram of damage development in type II laminates.

45